

# A mathematical model for the spread of multipartite viruses reveals their evolutionary potential

Eugenio Valdano<sup>1</sup>, Susanna Manrubia<sup>2,3</sup>,  
Sergio Gómez<sup>1</sup>, and Alex Arenas<sup>1</sup>

<sup>1</sup>Departament d'Enginyeria Informàtica i Matemàtiques, Tarragona, Spain.

<sup>2</sup>National Centre for Biotechnology (CSIC), Madrid, Spain.

<sup>3</sup>Grupo Interdisciplinar de Sistemas Complejos (GISC), Madrid, Spain.

## Abstract

Multipartite viruses replicate through a puzzling evolutionary strategy. These viruses have their genomes segmented into two or more parts encapsidated in separate particles that propagate independently. The requirement of host co-infection to complete the viral cycle represents a major drawback of this adaptive strategy, while its advantages remain unclear. Still, multipartitism is a successful adaptive solution observed in over 40% of all known viral families, particularly targeting plants. The transition from a monopartite to a bipartite viral form has been described in vitro under conditions of high multiplicity of infection, suggesting that cooperation between defective mutants is a plausible evolutionary pathway towards multipartitism. Here we devise a compartmental model for the spread of a multipartite virus in a population of hosts through vector mediated contacts. Our goal is to disentangle which mechanisms might favor the ecological emergence and persistence of multipartitism. Our analytical and numerical results uncover a rich phenomenology driven by the interplay between viral dynamics, vector driven mobility, and the structure of the host population. In the framework of our model, multipartitism appears as a successful adaptive strategy driven by mobility, that permits the colonization of environments forbidden to the nonsegmented variant. Surprisingly, this is promoted in homogeneous contact networks, which corresponds to the vast majority of farmed plant patterns. This is also in line with the observed rising of multipartitism concomitantly with the agricultural expansion.

Viruses transport their genetic material inside a protein shell, the capsid, surrounded in some species by a lipid membrane. In most viral species, each viral particle contains all the genetic material needed to carry out replication inside a host cell and to generate a progeny of viral particles. The main exception to this behaviour is found in multipartite viruses, first described in the 1960's [1]. These viruses have a genome segmented in two or more parts and, according to current evidence, the segments are encapsidated separately and propagate independently [2, 3]. As of today, there is no mainstream theory able to explain the adaptive advantage of such a strange lifestyle [4]: The main puzzle regarding multipartite viruses is how the requirement for co-infection, which imposes severe restrictions on the number of viral particles that have to simultaneously infect a susceptible host, is balanced by other adaptive advantages of multipartitism [5].

Up to 40% of all known viral families are multipartite. A large majority infects either plants or fungi, with only four known examples of species infecting exclusively animals [5]. Evolutionary pathways leading to multipartitism are likely multiple, since this strategy is present in RNA and DNA viruses, and in the latter case an origin to a single ancestral virus cannot be traced. Multipartitism is thus a widespread strategy with particularly high impact in crops and cultivars: many multipartite viruses are pathogenic, and their spread in new hosts can come with important economic consequences [6]. Actually, an evolutionary radiation in the diversity of multipartite viral species, many being just centuries old, was likely promoted by an intensification of agricultural practices [7]. It has been put forward that multipartite species might be at an advantage in the face of environmental changes, since they likely adapt faster due to the high plasticity conferred by their genomic architecture [5].

The wild-type (*wt*) form of a virus is the one containing the full genome [8]. Defective variants of the wild-type form might emerge as replication errors and thrive under conditions that ensure a high multiplicity of infection (MOI) [9, 10]. It has been shown *in vitro* that two defective forms spontaneously generated by foot-and-mouth disease virus (FMDV has an unsegmented genome formed by ssRNA of positive polarity), can complement each other and substitute the wild-type form in short time [11]. This strategy has been formally explored in models of competitive dynamics between the *wt* and a number of complementing segments [12], which implemented different advantages that could compensate for the cost of an increased MOI. The model mimicked the experimental setting where, in particular, host availability corresponded to that of a well-mixed system. Two of the advantages implemented had been theoretically proposed in the past thought, as of yet, have not received empirical support (a faster replicative ability [13] and a slower accumulation of deleterious mutations in shorter segments [14, 15]) while, in the case of FMDV, it was shown that capsids containing shorter genomes enjoyed a larger average lifetime between infection events [16]. This differential degradation dependent on genome length was sufficient to compensate for co-infection requirements in multipartite forms with two to up to four segments [12].

The rise and persistence of multipartite viral forms, and especially the features that characterize its epidemic spread, have not been addressed so far in a more realistic ecological context. Actually, it is intriguing that the burst of multipartite diversity coincided with the expansion of agriculture. From the viewpoint of networks of contacts between potential hosts, the latter signals a relevant transition between a situation where hosts were scattered and perhaps hierarchically clustered, experiencing heterogeneous contacts, to a new

situation where the network of contacts became highly homogeneous and short-ranged. Here we tackle this issue through a compartmental model for the spread of a virus circulating as *wt* together with a cohort of defective, and potentially complementary, mutants. Using both analytical calculations and numerical tools, we derive the conditions under which multipartite forms grow in abundance and persist in the host population. Since no apparent structural feature discriminates multipartite viruses from monopartite ones –as they are found exhibiting different capsid structures, genome sizes and types [17]– we include in the model as few virological features as possible, and investigate how multipartitism might persist solely as a result of host-pathogen dynamics.

In an ecological context, a first mechanism for the resilience of multipartitism is differential degradation (or the formally equivalent advantages of faster replication or elimination of deleterious mutations through sex) which takes the form of a difference between-host transmissibility of the defective variants with respect to the *wt*. A second biological mechanism encoded by transmissibility is the mode of transmission of multipartite viruses between hosts. Most known multipartite viruses are spread by vectors (mainly insects), which typically pick up very few viral particles from an infected plant [18]. The transmission process between hosts typically acts as a population bottleneck for the virus, entailing a loss of genetic diversity and, if severe enough, the systematic purge of deleterious forms [19]. Any of the mentioned mechanisms differently affect the chances of the *wt* or defective particles to reach the target hosts, leading to a difference in transmissibility. A single model parameter, therefore, tunes the relative transmissibility and embraces a number of different biological processes. In this sense, the results of our model can be extended to other systems as long as the specific mechanisms involved in their propagatory success can be cast in the form of changes in transmissibility.

Alongside the biological properties of the virus, the model implements the structure of contacts among susceptible hosts. For a majority of multipartite viruses, this means the contact network induced by vector movements among plants. Its topology may be diverse, depending on plant distribution and vector behavior, with two limit cases being the distribution of plant species in the wild (see, e.g.[20] and references therein) and huge modern agriculturally homogeneous regions [21]. These different architectures are implemented through homogeneous and heterogeneous contact rates, which allow us to highlight the role of different topologies in the persistence of viruses in different forms.

## The epidemic model

We consider a large population of  $N$  hosts susceptible to a virus that may circulate in its *wild-type* (*wt*) form together with  $v$  segmented and defective variants. As previously done [12] we apply a separation between evolutionary and ecological scales such that we do not explicitly model the mutation events affecting the *wt*, and assume that  $v$  possible segments exist as initial condition. These segments, when simultaneously present in the host, complement each other and are able to complete the virus infective cycle in the absence of the *wt*.

As customary in compartmental models, we consider that hosts are either free of the virus, and thus susceptible (S), or infected (I) by a certain combination of the viral forms, translating into various infectious compartments (Fig. 1). The main assumption is that a host can be infected only by a combination that guarantees the presence of the full

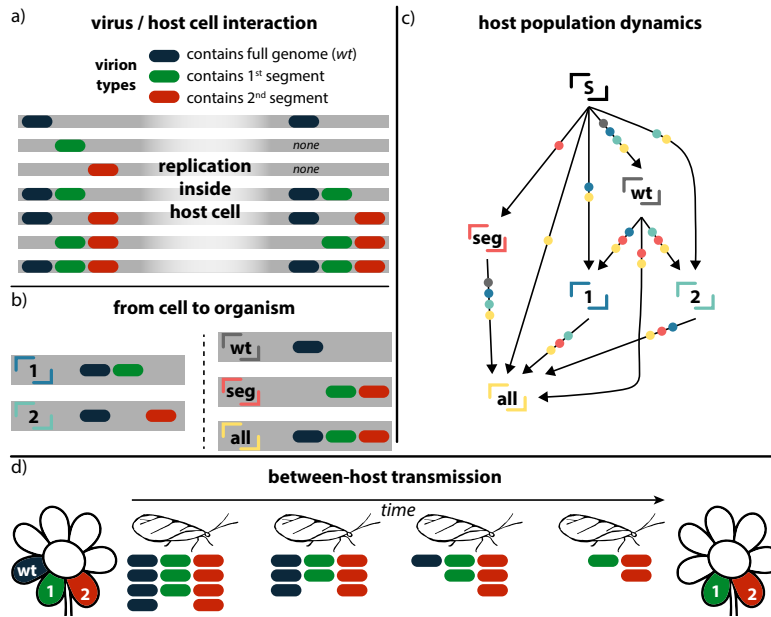


**Figure 1:** Schematic illustration of multipartite viral dynamics and our modeling framework. For simplicity's sake we focus here on a bipartite virus. (A) describes the different viral species circulating, and their replication dynamics inside a host cell. In each line line, the viral particles infecting the same host cell are shown on the left, and the product of replication on the right. (B) describes the different infectious compartments of the compartmental model at the population level, in terms of the viral species they are infected by. In (C) we outline the compartmental model of a bipartite viruses. An arrow going from one compartment to another means that a host finding itself the former can become the latter by coming into contact with one of the compartments marked as dots on the arrow itself. Rates specific to each interaction are not shown. Recovery, by which each infectious compartment turns Susceptible at a rate  $\mu$  is not shown, either. (D) depicts the transmission of the virus from host to host in terms of vectors. The vector picks up some viral particles of different variants (represented below it). During the time it takes for it to reach another plant, these particles degrade. One hypothesis behind differential transmissibility is differential degradation, here depicted. Lower degradation rates due of the defective variants lead to a chance of transmission higher than wt.

genome. Without it, we consider that no systemic infection is possible. Moreover, we assume that host cells replicate all, and only, the viral forms they are infected by (Fig. 1A). These assumptions determine the set of existing compartments.

Two compartments are present regardless of the value of  $v$ . They are  $\lceil \mathbf{wt} \rceil$  and  $\lceil \mathbf{all} \rceil$ , and identify plants infected by the  $wt$  only, and by the  $wt$  together with all the  $v$  variants, respectively. If  $v = 1$ , no other compartments exist. If  $v > 1$ ,  $\lceil \mathbf{seg} \rceil$  identifies plants infected by all the  $v$  defective and complementing variants, without the  $wt$ . In addition, there are  $2^v - 1$  other compartments containing  $wt$  plus a combination of some (not all) of the defective variants. We name them according to which of the latter they are infected by. For instance,  $\lceil \mathbf{1} \rceil$  contains  $wt$  plus variant 1, and  $\lceil \mathbf{35} \rceil$  contains  $wt$  plus variants 3 and 5. If defective variants are not present,  $\lceil \mathbf{wt} \rceil$  behaves like a standard Susceptible–Infected–Susceptible (SIS) model, with probability of transmission upon contact equal to  $\lambda$ .

We implement enhanced transmissibility of defective variants by assuming they spread with a probability  $\rho\lambda$ .  $\rho = 1$  thus means that  $wt$  and segments are epidemiologically equivalent, while any value larger than 1 causes the defective variants to transmit more easily than the  $wt$ . For a graphic representation of the spreading route and differential transmissibility see Fig. 1D. In the general case, an agent in a given compartment may transmit some (or all) the viral species it hosts to the one it is in contact with, with a probability depending on the initial compartments of the two agents, and the final compartment. For instance, a host in compartment  $\lceil \mathbf{1} \rceil$ , upon contact with a susceptible one, may transmit both  $wt$  and 1, turning the susceptible into a  $\lceil \mathbf{1} \rceil$ , or just the  $wt$ , turning it into a  $\lceil \mathbf{wt} \rceil$ ; variant 1 cannot be transmitted without the  $wt$ , as stated. A schematic representation of the compartmental model for a bipartite virus ( $v = 2$ ) is depicted in Fig. 1C.

In agreement with current evidence, we assume that the different species of viral particles transmit independently, so that the probability of concurrent transmission of two variants (and  $wt$ ) is simply the product of the probabilities of the single events. We also assume that co-infection by  $wt$  and variants does not alter the infectious period, allowing us to model recovery at a rate  $\mu$  for all infected hosts.

When the virus is introduced into a susceptible population, it can either die out quickly and leave the system disease-free (disease-free state, **dfs**), or reach endemicity. There are four possible endemic states, depending of which variants circulate. We equivalently use the term *equilibria*, as they are the stable equilibrium points of the spreading dynamics. The first one is **wt**, in which only the  $wt$  is prevalent, and the defective variants have died out. This case maps into an effective SIS model for the compartment  $\lceil \mathbf{wt} \rceil$ . In the second one, **hj**, any defective segment can circulate alongside the  $wt$  because, roughly speaking, the transmissibility of the latter is so high that any defective variant can hijack it, with no need to complement the genome with other variants. In this case, we will likely see the circulation of a number of variants lower than  $v$ , as segments can go extinct without hampering the circulation of the remaining ones. The third endemic state, **seg**, witnesses the presence of all and exactly the  $v$  segmented variants without  $wt$ , and in this case complementation is essential. This state is a SIS model for the compartment  $\lceil \mathbf{seg} \rceil$ . Finally, the state **all** exhibits circulation of the  $wt$  plus all the variants  $v$ . The epidemic phases of the disease are then defined in terms of which of these endemic states they allow. Above the epidemic threshold, i.e., when equilibria other than **dfs** exist, there are five

possible phases: *wt*-phase allows only **wt**; *contingent*-phase allows **wt**, **hj** and **all**; *mix*-phase allows **wt**, **seg** and **all**; *seg*-phase allows only **seg**; finally *all*-phase admits all the possible endemic states. Figure 2 provides a schematic representation of the relationship between phases and endemic states.

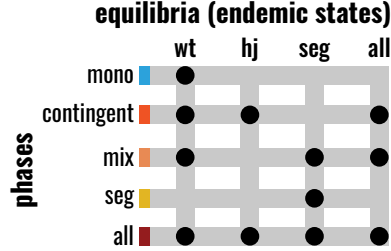


**Figure 2:** Connection between phases and endemic states. This figure provides a connection between the possible phases of the epidemic and the endemic states they allow. A black dot connecting a phase and an endemic state means that the latter is a stable equilibrium in that phase, and can occur.

In the following, we analytically derive the critical surfaces that separate the different phases in the space of the parameters. This means that, given specific values of the parameters, it will be possible to predict the possible outcome of the spread, thus characterizing the conditions leading to the persistence of multipartitism, and which kind. Then, using numerical simulations, we will study the endemic prevalences of the endemic states, and their probability of occurring, for a representative set of parameter values.

Firstly, however, we need to set up the theoretical modeling framework in terms of reaction-diffusion equations. For a generic  $v$ , we order the compartments by increasing number of viral species they contain, starting from  $\lceil \text{wt} \rceil$ , and ending with  $\lceil \text{seg} \rceil$ ,  $\lceil \text{all} \rceil$ . For instance, for  $v = 3$ , this would be  $\lceil \text{wt} \rceil$ ,  $\lceil 1 \rceil$ ,  $\lceil 2 \rceil$ ,  $\lceil 3 \rceil$ ,  $\lceil 12 \rceil$ ,  $\lceil 13 \rceil$ ,  $\lceil 23 \rceil$ ,  $\lceil \text{seg} \rceil$ ,  $\lceil \text{all} \rceil$ . Within the framework of heterogeneous mean field [22, 23, 24], we divide hosts in classes according to their contact potential (*degree* in the language of networks), so that if two hosts have degree  $k, h$ , respectively, their contact rate will be the product  $kh$ . We assume hosts with the same degree are equivalent, and consider the prevalence per degree class. To this end, we define the variable  $x_\nu^k$  as the prevalence of compartment with index  $\nu$  and degree class  $k$ , i.e., the fraction of the host population which has that degree, and finds itself in that compartment. In terms of  $x_\nu^k$ , the equations describing the evolution of the disease are

$$\dot{x}_\nu^k = -\mu x_\nu^k + \frac{k}{\langle k \rangle} \sum_\beta \left( \sum_h h p_\gamma(h) x_\beta^h \right) \left[ \Gamma_{\nu\beta} \left( 1 - \sum_\sigma x_\sigma^k \right) + \sum_\sigma \Lambda_{\nu\beta\sigma} x_\sigma^k \right]. \quad (1)$$

$p_\gamma(k)$  is the probability of a host having degree equal to  $k$ . We consider the *homogeneous* case, where all hosts have the same degree, so that  $p_\gamma(k) = \delta_{k,1}$  (with no loss of generality we set it to 1), and a highly *heterogeneous* case, where  $p_\gamma(k) = C_\gamma k^{-\gamma}$  is a power-law with exponent  $\gamma$ , and normalization constant  $C_\gamma$ .  $\Gamma_{\nu\beta}$  is the rate of the transition  $\lceil \beta \rceil \lceil \text{S} \rceil \rightarrow \lceil \beta \rceil \lceil \nu \rceil$ , i.e., a transition affecting the prevalence of compartment  $\lceil \nu \rceil$  through a contact between a host in compartment  $\lceil \beta \rceil$  and a Susceptible.  $\Lambda_{\nu\beta\sigma}$  encodes transmission rates among infected individuals, and specifically a transmission from  $\lceil \beta \rceil$  to  $\lceil \sigma \rceil$ , that leads to the change of the prevalence of  $\lceil \nu \rceil$ . The entries of  $\Gamma_{\nu\beta}$ ,  $\Lambda_{\nu\beta\sigma}$  are functions of  $\lambda$ ,  $\rho$  and  $v$ .

The analytical approach to computing the critical surfaces consists in studying the linear stability of the different equilibria of Eq. (S.1). In order to compute the prevalence values and occurrence probability of these equilibria, we also resort to stochastic spreading simulations. The extensive calculations are reported in Methods and SI, as well as the explanation of the numerical simulations.

## Results and Discussion

### Critical behavior

The five phases are completely determined by three surfaces, whose analytical expression we compute. They are  $T_1$ , above which the  $wt$  can spread on its own (epidemic threshold for the compartment  $\lceil wt \rceil$  while alone);  $T_2$ , above which segments circulate by hijacking the  $wt$ , and  $T_s$ , which is the epidemic threshold for the compartment  $\lceil seg \rceil$  circulating alone. The expressions we find are

$$T_1 = \{\lambda = \hat{\mu}\}; \quad (2)$$

$$T_2 = \left\{ \lambda = \frac{1+\rho}{\rho} \frac{\hat{\mu}}{1+\hat{\mu}} \right\}; \quad (3)$$

$$T_s = \left\{ \lambda = \frac{\hat{\mu}^{1/v}}{\rho} \right\}. \quad (4)$$

$\hat{\mu}$  is an effective recovery-rate encoding both the actual recovery rate, and the topology of the contacts:  $\hat{\mu} = \mu \langle k \rangle / \langle k^2 \rangle$ . Given that homogeneous contact networks have  $\langle k \rangle \sim \langle k^2 \rangle$ , the heterogeneous (power-law-like) network recovers the homogeneous case when  $\gamma \rightarrow \infty$ . Hence, the smaller the exponent  $\gamma$ , the more heterogeneous the contact network is, roughly meaning that there is a higher chance of encountering hosts that, having a lot of connections, act as superspreaders and are able to reach a consistent part of the population. Moreover, we remark that for an exponent  $2 < \gamma < 3$ ,  $\hat{\mu}$  goes to zero ( $\hat{\mu} \rightarrow 0$ ) in the limit of large population. This implies not only that  $T_1$  goes to zero, as it is well-known [22], but that  $T_2, T_s$  do it as well. However, while  $T_2/T_1$  remains finite as  $\hat{\mu}$  goes to 0, meaning that  $T_1, T_2$  go to zero with the same speed, we find that  $T_s/T_1 \rightarrow \infty$ . This implies that  $T_s$  goes to zero more slowly and, the higher  $v$  is, the more slowly it does.

The study of Eq. (2,3,4) reveals four regimes. For low or zero differential transmissibility ( $\rho < \hat{\mu}^{-(v-1)/v} - (1 - \hat{\mu}^{1/v})$ ), as  $\lambda$  increases, one crosses the *mono*-phase, then the *contingent*-phase and finally the *all*-phase (see Fig. 3(A)). For intermediate values of differential transmissibility ( $\hat{\mu}^{-(v-1)/v} - (1 - \hat{\mu}^{1/v}) < \rho < \hat{\mu}^{-(v-1)/v}$ ), the *mix*-phase substitutes the contingent phase. This can be seen in plots Fig. 3(B,C). Then, when  $\hat{\mu}^{-(v-1)/v} < \rho < \hat{\mu}^{-1}$ , increasing  $\lambda$  causes the system to be in the *seg*-phase, followed by the *mix*-phase and later by the *all*-phase (see Fig. 3(B,C,D)). Finally, for very high differential transmissibility  $\rho > \hat{\mu}^{-1}$ , the  $wt$  no longer spreads and the only possible phase is the *seg*-phase (see Fig. 3(B,C)).

### Endemic prevalences

For any possible value of the parameters, Eq. (2,3,4) tell us which endemic states are possible, i.e., which prevalences are higher than zero. They provide, however, no information

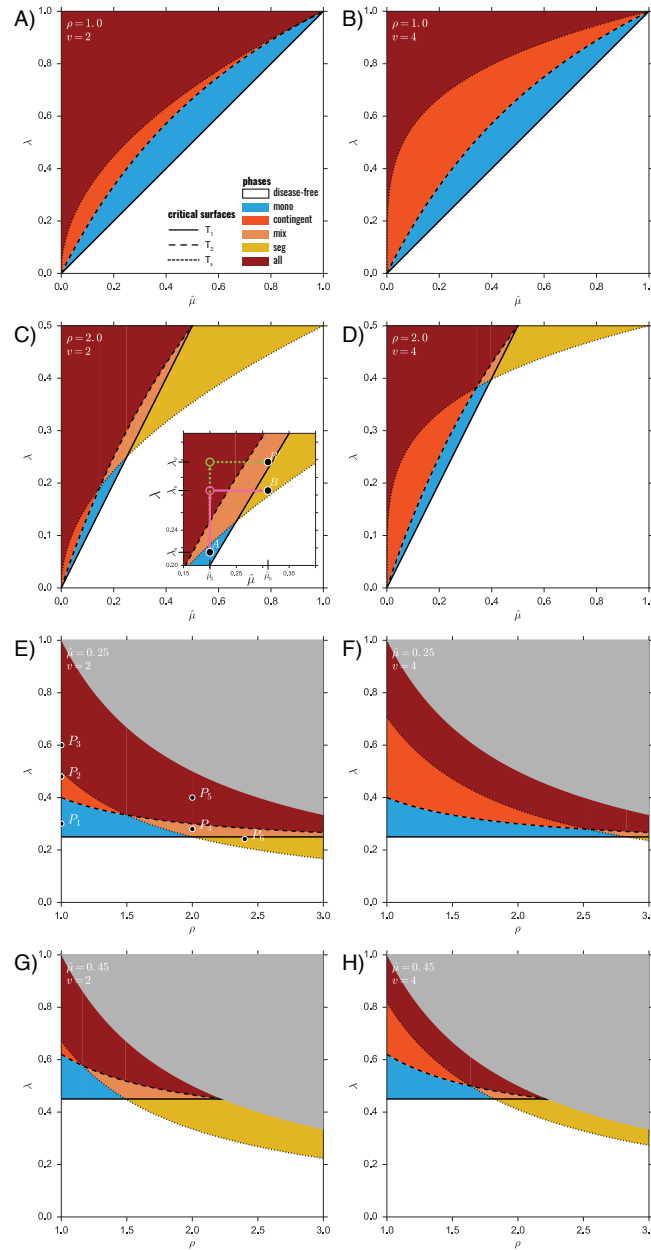


**Figure 3:** Parameter exploration and endemic phases. Of the four parameters that influence the critical points  $(\hat{\mu}, \lambda, \rho, v)$ , two are in turn kept fixed and the remaining two explored in a two-dimensional plot highlighting the different phases. The value of the fixed parameters is reported on the top left of each plot. The y-axis of each plot is always the transmissibility of  $wt$  ( $\lambda$ ). The critical surfaces are  $T_1, T_2, T_s$  (solid, dashed, dotted lines), and the phases are colored as in legend. The gray areas mark forbidden parameter values (probabilities higher than 1). The inset in (C) is a magnification of a subregion of the (C) plot. In (E) the points displayed have the following values:  $P_1 = (1, 0.3)$ ,  $P_2 = (1, 0.48)$ ,  $P_3 = (1, 0.6)$ ,  $P_4 = (2, 0.28)$ ,  $P_5 = (2, 0.4)$ ,  $P_6 = (2.4, 0.248)$ .



about the values of such prevalences, which are, in principle, the solutions of the algebraic system obtained by setting  $\dot{x}_\nu = 0$  in Eq. (S.1). A closed-form solution of this system does not exist for heterogeneous networks. In the homogeneous case, while a complete analytical derivation of the endemic states is not possible, we can obtain two important results. Firstly, we notice that the total prevalence of the  $wt$ , i.e., the fraction of hosts infected by it ( $z = \sum_{\nu \in \Gamma_{\text{seg-}}} x_\nu$ ), obeys an SIS dynamics (see SI - Sec. 5) with transmissibility  $\lambda$ , and can thus be computed as  $z_{wt} = 1 - \mu/\lambda$ . Secondly, when the whole set of segments circulates without  $wt$  (as compartment  $\Gamma_{\text{seg-}}$ ), again the virus spreads as an SIS, this time with transmissibility  $(\rho\lambda)^v$ , and its endemic value can be predicted in the same fashion:  $z_{seg} = 1 - \frac{\rho}{(\rho\lambda)^v}$ . Interestingly, for high  $\rho$ , and a transmissibility  $\lambda > \rho^{-v/(v-1)}$ , it turns out that  $z_{seg} > z_{wt}$ : the prevalence of the multipartite form is higher than that of the  $wt$ .

In order to fully characterize the endemic states, we resort now to stochastic spreading simulations (see Methods), focusing on the bipartite case ( $v = 2$ ). A higher number of variants ( $v > 2$ ) would not change the qualitatively picture: It would simply increase the possible values for the prevalence of **hj** by increasing the number of possible segments that survive through hijacking. We choose six points in the parameter space that lie in different phases (see Fig. 3(E)), and for those values we carry out the simulations.

### Homogeneous contact networks

We firstly focus on homogeneous contact networks. The results are shown in Fig. 4(A). We characterize the endemic states in terms of their type (Fig. 2), and plot their total prevalence, and the prevalence of the defective variants. The former is the fraction of hosts infected by any configuration of the virus, and the latter is the fraction infected by at least one defective variant. In the points lying on the  $x$ -axis (labeled by **wt**) the defective variants have gone extinct, and the  $wt$  behaves like an SIS (states **wt**). The points lying on the diagonal have witnessed the extinction of the  $wt$ , and the defective variants are circulating together in the  $\Gamma_{\text{seg-}}$  compartment (states **seg**). Their values match the theoretical prediction (dashed vertical lines). The solid vertical lines in Fig. 4(A) are the theoretical predictions of  $wt$  prevalence. They match all equilibria of type both **wt** and **hj**, as in those cases the total prevalence coincides with the prevalence of the  $wt$ . The states **all**, whose total prevalence cannot be predicted analytically, have the highest prevalence. This picture further confirms the relationship between the theoretically predicted phases and the allowed endemic states (Fig. 3(D)).

### Heterogeneous contact networks

Previously we have stated that the critical surfaces are not sensitive to recovery rate and topology separately, but only to the parameter  $\hat{\mu}$  encoding both at the same time. Specifically, two populations with different recovery rate and contact heterogeneity, but with the same  $\hat{\mu}$ , are indistinguishable from the point of view of their critical behavior. The endemic prevalences, however, break this symmetry, as one can see from Fig. 4(B), where we focus on  $P_3$  (Fig. 3(D)) and get to  $\hat{\mu} = 0.25$  both with a homogeneous network (as in Fig. 4(B)), and with two heterogeneous networks with exponent  $\gamma = 3.5$  and  $\gamma = 3.2$ . All the three configurations show all the equilibria, as expected by the critical behavior, but in the heterogeneous case the prevalence is consistently lower for each equilibrium.

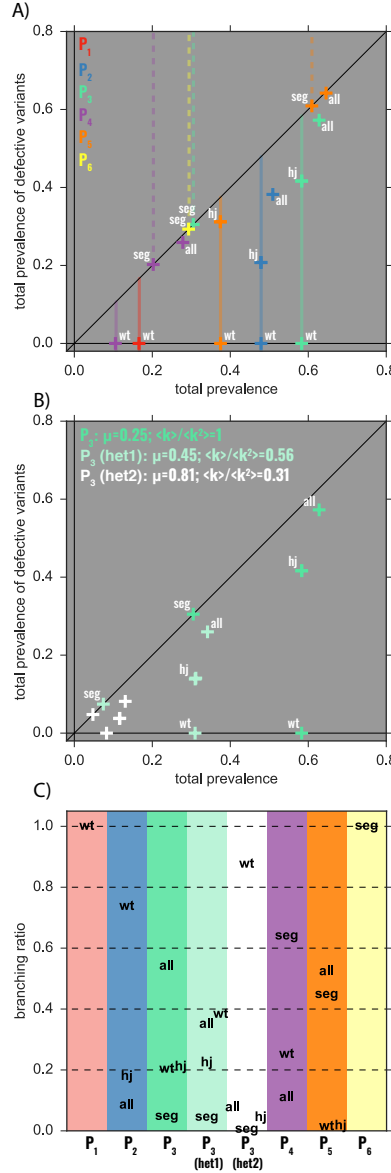


**Figure 4:** Endemic states. Plots (A,B) show the results of the simulations for the endemic states of configurations corresponding to the points in Fig. 3(E), for a bipartite virus ( $v = 2$ ). In both (A) and (B), x-axis is the total prevalence of the disease, i.e., the fraction of hosts infected by any configuration of the virus, at equilibrium. The y-axis is the prevalence of the defective variants, i.e., the fraction of hosts infected by at least one defective segment. The points are numerically recovered endemic states, their type being indicated by the labels. In (A) the underlying contact network is homogeneous, so that  $\hat{\mu} = \mu = 0.25$ . The solid vertical lines mark the analytical prediction of the total prevalence when wt is present either alone or together with just one variant. The dashed vertical lines mark the analytical prediction of the prevalence when the segments circulate without wt. The crosses mark the prevalence values of the equilibrium points averaged over the runs not leading to extinction, among the 5000 executed per point. (B) focuses on  $P_3$  (in Fig. 3(E)): the fixed value  $\hat{\mu} = 0.25$  is obtained either as  $\mu = \hat{\mu}$  (homogeneous network, as in (B)), or with two heterogeneous networks with exponent  $\gamma = 3.5$ ,  $\mu = 0.45$  and  $\gamma = 3.2$ ,  $\mu \approx 0.81$  (and thus  $\langle k \rangle / \langle k^2 \rangle \approx 0.56$  and  $\langle k \rangle / \langle k^2 \rangle \approx 0.31$ , respectively). For each of the points and the equilibria examined, (C) reports the branching ratio, defined as the probability of reaching that particular equilibrium. They are computing by starting all the simulations with all susceptible but one in 'all' (infected by wt and all the variants), and counting the fraction of the runs that reach that equilibrium, among the ones that do not go to extinction.

## Sensitivity to initial conditions: branching ratios

Up to now, we have identified the phases (allowed endemic states) and computed the prevalence of such states. We now focus on the probability of occurrence of each state. For each of the usual points in Fig. 3(E), we show the probability of reaching each equilibrium in Fig. 4(C). This is achieved by counting the number of stochastic realizations that, starting from similar initial conditions, lead to that specific equilibrium (*branching ratio* of that equilibrium). Clearly, points  $P_1$  and  $P_6$  have only one endemic state, which has branching ratio equal to one. For the other points, which have more than one endemic state, the branching ratios are more informative, as they tell us which epidemic scenarios are more likely to happen in case of disease introduction. With one caveat, however: while both the critical behavior and the prevalence of the endemic states are inherent properties of the system that do not depend on the specific initial conditions chosen, this is not true for the branching ratios, which are clearly influenced by the initial infection status of the population. Given that, however, we computed them by seeding only one host in the  $\lceil \text{all} \rceil$  compartment to a susceptible population, we can say that our branching ratios are—at least qualitatively—reliable in an invasion scenario, in which the disease is introduced in the population by just one (or few) individuals, and one is interested in studying the impact of this bottleneck on viral evolution.

Interactions among different pathogenic agents have been widely studied in the past, through both methodological and applied works [25, 26, 27, 28, 29]. Those studies have always assumed that the pathogens involved can spread on their own, which is not the case for defective forms or for the pieces of a multipartite virus. Also, in the latter case interactions occur between akines, causing a non-trivial evolutionary game that involves competitive as well as cooperative strategies.

## Rise of multipartitism

Using the analytical characterization of the endemic phases and the numerical study of the equilibria, we now can investigate under which conditions the interplay between the spread of the virus and the topology of contacts lead to the emergence and persistence of multipartitism. For the sake of simplicity, we start by considering no differential transmissibility ( $\rho = 1$ ): *wt* and segments have the same transmission probability. The relevant figures are Fig. 3(A,B), points  $P_1, P_2, P_3$  in Fig. 3(E) and Fig. 4. In this scenario, three phases are possible, and one crosses them all by increasing the transmissibility  $\lambda$ . The first one ( $\lambda$  just above  $T_1$ ) is the *wt*-phase, in which only the *wt* can circulate, and whenever a defective segment is produced, it quickly goes extinct. By increasing  $\lambda$ , we then encounter the *contingent*-phase. This phase predates the appearance of true multipartitism, as defective segments can hijack the *wt* to circulate. These segments cannot persist on their own, but the highly prevalent *wt* allows them to complete the replication cycle. At this stage, any defective segment is a *commensal* of *wt*, as the persistence of the former depends on the latter, while *wt*'s fitness remains unchanged. The emergence of multipartitism in this context is a contingent process: segments circulate simply because it is allowed, causing no change to the overall fitness of the virus. Furthermore, there is no selective pressure towards complementation, as a combination of segments reconstructing the full genome without the presence of the *wt* (compartment  $\lceil \text{seg} \rceil$ ) would not be able to persist.

A further increase in  $\lambda$  takes us to the *all*-phase. Here, in addition to the commensal re-

relationship between *wt* and segments, complementing variants are able to circulate on their own, without *wt*: the equilibrium **seg** emerges. Selection then imposes a bias on those segments that together reconstruct the genome, as they represent a new effective spreading configuration, and increase the overall viral fitness. They are thus advantaged with respect to purely commensal segments. This fitness-enhancing effect is quite straightforward: let us suppose that, due to viral or host population bottlenecks, or another stochastic event, *wt* prevalence goes down drastically, to the point where it is cleared from the system. In the *contingent*-phase this would lead to complete viral extinction, as all the segments would die out, too, as their persistence is linked to *wt*'s. In the *all*-phase, on the other hand, the virus is more resilient, as it can still circulate thanks to complementation.

The interplay of these diverse evolutionary processes shape both  $T_2$  and  $T_s$  (Eq. (3,4)). The former does not depend on the required number of complementing variants ( $v$ ), because each segment can hijack the *wt* independently of the others. The latter, on the contrary, increases exponentially with  $v$ , as the probability of being co-infected by all the variants depends on their number. This is qualitative agreement with results in [12], where it was shown that the larger the number of segments, the harder to reach the persistence of the segmented variants within a host.

## The *contingent*-phase acts as a stepping stone towards multipartitism

The analysis of the prevalences (Fig 4(A)) confirms the evolutionary drivers behind the different phases, and adds information regarding crossed effects between viral types. Let us focus on the *contingent*-phase (point  $P_2$  in Fig 4(A)), and the **all** state. The total prevalence of the latter state is higher than **wt**'s and **hj**'s in the same phase, implying that some hosts are infected by complementing segments without *wt* (compartment  $\lceil \text{seg} \rceil$ ), that is by a *bona fide* multipartite virus. Given that the multipartite form is not endemic in this phase—the *contingent*-phase relies on the *wt* for viral persistence—, this excess prevalence of the **all** state is a by-product of overall viral prevalence, rather than its driver: an extinction of the *wt* would quickly drive segmented variants to extinction. It is, however, and important one, as while it may not increase fitness in that specific environment, it permits for the independent replication of the set of complementing variants; these are then able to invade other environments in which the *wt* could not persist, as we will see in the following.

## Increased heterogeneity of the contact network impairs multipartitism

Let us examine the effect of a heterogeneous contact network on the phases and equilibria above. As we have explained, in the phase space, topology is encoded in the parameter  $\hat{\mu}$ . A low epidemic threshold is a well known feature of heterogeneous networks [22, 23, 30]. Specifically, scale-free networks with  $\gamma < 3$  exhibit a vanishing threshold as they grow bigger, as the emergence of highly connected hubs ensures the persistence of the disease at any value of transmissibility, that is  $\langle k \rangle / \langle k^2 \rangle \rightarrow 0$  (and as a result,  $\hat{\mu} \rightarrow 0$ ) as the number of potential hosts grows,  $N \rightarrow \infty$ . In our case this translates into  $T_1$ , which is the epidemic threshold, going to zero for  $\hat{\mu} \rightarrow 0$ . Also  $T_2, T_s \rightarrow 0$ . Further information is

obtained when comparing their limit behaviors. As  $\hat{\mu}$  becomes smaller,  $T_2/T_1$  increases but remains finite, while  $T_s/T_1 \rightarrow \infty$ . This implies that, the higher the heterogeneity of the network, the more difficult it becomes for multipartitism to persist. Specifically, reaching the *all*-phase from the *mono*-phase would require an infinite relative increase (in the limit  $\hat{\mu} \rightarrow 0$ ) in transmissibility. Even when heterogeneity is not severe enough so as to cause the threshold to vanish, i.e., when  $\gamma > 3$ , heterogeneity makes it harder to sustain multipartitism, as both  $T_2/T_1$  and  $T_s/T_1$  are decreasing functions of  $\hat{\mu}$ .

Heterogeneity also modifies endemic prevalences and the branching ratios of equilibria. Let us examine point  $P_3$  (*all*-phase in Fig. 3(E)): when the network is homogeneous, the highest branching ratio corresponds to **all**, and the equilibria containing segments together (**hj**) happens 20% of the times. When the network is heterogeneous, this fraction decreases, and **wt** quickly overtakes **all** in being the most probable outcome.

Summarizing, homogeneous contact patterns favor the emergence and persistence of multipartitism, while heterogeneous contacts hamper it. Qualitatively, this is the result of the complex interaction between the bottlenecks induced by between-host transmission and the presence of superspreaders, i.e., hosts that can potentially infect a large fraction of the population thanks to their high number of contacts. Combining this mechanism with a low MOI –and hence low  $\lambda$ – may help explain the evolutionary radiation of multipartite viral forms linked to the increase of agricultural practice. In crops and cultivars, contacts among hosts are much more homogeneous (and often closer) than in wild settings, tremendously alleviating the requirements imposed by co-infection. Multipartite viruses adapted to the patchy distribution of wild hosts could have found it easy to propagate in regular, monospecific host populations which in all cases have closely related wild forms from which they departed through artificial selection [31].

## An increased transmissibility of segmented forms induces additional phases facilitating multipartitism

Increasing the transmissibility of the segments with respect to that of the *wt*'s ( $\rho > 1$ ) facilitates the circulation of the virus in the form of complementing segments. As  $\rho$  increases, the endemic state **seg** becomes more prevalent and more likely with respect to **wt** (see Fig. 4(C,D)). Specifically, the value of the transmissibility for which  $z_{seg} > z_{wt}$  decreases as  $\rho$  increases, facilitating the predominance of the multipartite form (in Fig. 4(A) point  $P_3$  has  $z_{wt} < z_{seg}$ , while  $P_4, P_5$   $z_{seg} > z_{wt}$ ). Most importantly,  $\rho > 1$  causes two new phases to emerge (Fig. 4(B-D)), and both facilitate the rising of multipartitism by eliminating **hj** from its possible equilibria. One is the *mix*-phase, in which the virus circulates either as *wt* or as a multipartite. The *mix*-phase also presents an **all** endemic state that results from the interaction between the two former equilibria. Now, it is not a commensal relation, like in the *all*-phase. The second emerging phase is the *seg*-phase, in which only the complemented multipartite virus is able to circulate, while the monopartite version quickly goes extinct (yellow, and point  $P_6$  in Figs. 3, 4). This phase is of paramount importance because it lies in a parameter region where, without developing multipartitism, the virus would not be endemic. It exemplifies multipartitism as a successful adaptation of the virus to the environment.

## Implications for the emergence of multipartitism in natural scenarios

The simultaneous presence of monopartite and defective-complementing forms of the same virus has only been observed *in vitro* [32, 33, 34, 11]. *In vivo*, viral species circulate either as monopartite, or as multipartite, i.e., in the endemic states **wt** and **seg**. Also, though many defective viral forms are generated and detected *in vitro* co-propagating with the wild type (which would correspond to an *in vitro* **hj**), this equilibrium is rarely found in wild plants. There is, however, an association between fully-fledged viruses and defective viral forms formally equivalent to the **hj** equilibrium: virus and viral satellites [35]. Often, and in contrast with the situation described in this work, satellites modify the aetiology of viral infections [36], such that the transmissibility and the recovery rate might be affected by its presence in no particular direction. There are other classes of hyperparasites that depend on a functional virus for replication (e.g. virophages [37] or viroid-like satellites [38]) whose ecological dynamics could, with appropriate modifications, be described in the framework discussed here. Interestingly, it has been proposed that virus-satellite associations, a typically unrelated tandem from a phylogenetic viewpoint, might evolve towards full co-dependence, and therefore be a possible, alternative evolutionary pathway to multipartitism [5].

Though our knowledge of viral phenomenology is still limited and likely biased [39], our results indicate that endemic states mixing monopartite and multipartite cognate forms (**hj**, **all**) need values of transmissibility difficult to sustain: endemicity can be achieved with lower values of transmissibility if the virus would be propagating only as a wild-type, while high values entail a cost that is usually compensated by decreasing infectivity [40].

Albeit rare, however, these endemic states might be a stepping stone towards multipartitism even if they are only transiently present, as in the following example. Consider a purely monopartite virus endemic in a plant population, in a specific area, with parameters  $\hat{\mu}_A$ ,  $\lambda_A$  as in point *A* in Fig. 3(E, inset).  $\hat{\mu}_A$  is a combination of the recovery rate of the disease (characteristic of the host-virus interaction), and the between-plant contact network, driven by plant distribution and vector movements. A second population, occupying an adjacent geographic area, may have a different parameter ( $\hat{\mu}_B > \hat{\mu}_A$ ), due to a different contact topology. As Fig. 3(E, inset) shows, the virus is able to colonize the second population only through an evolutionary process that increases its transmissibility up to at least  $\lambda_{B'}$ , so that point *B'* is above the epidemic threshold (green path). It is reasonable to assume that the larger the increase in transmissibility required, the less likely this process is, given that the required mutation(s) are less likely and possibly more costly to maintain. The emergence of multipartitism decreases the evolutionary distance between the two states, increasing adaptability (magenta path in figure). Random mutations, in fact, need to increase transmissibility from  $\lambda_A$  (*mono*-phase) to  $\lambda_B < \lambda_{B'}$  (*all*-phase), where a complementing, multipartite version of the virus can emerge. Invasion of the second population is now possible, because the new viral forms effectively lowers the epidemic threshold in  $\hat{\mu}_B$ , thanks to the emergence of the *seg*-phase (point *B*). This simplistic example not only shows that multipartitism can emerge as a fitness-enhancing feature, but also that coexistence of monopartite and multipartite forms is a key stage in the evolutionary process, albeit possibly transient and short-lived. This example also allows to elucidate the hampering effect of network heterogeneity on multipartitism. By increasing the dis-

tance between the *mono*-phase and the *all*-phase, network heterogeneity reduces the ratio  $\lambda_{B'}/\lambda_B$ , making multipartitism less advantageous. In conclusion, while making viral persistence overall easier, network heterogeneity curbs the potential of multipartitism as an effective adaptation strategy.

## Conclusion

Multipartitism represents an example of a complex and as-of-today puzzling viral behavior. We have developed a formal framework that, starting from few key biological features, can model multipartite viral dynamics, spread and persistence at host population level. Though we assumed that multipartitism arose through complementation between defective viral forms generated by the wild-type virus, as it has been observed *in vitro*, our results can be extended to other situations with relative ease. A main novelty of our study is the consideration of heterogeneous contact topologies among hosts that mimic their *in vivo* distribution. We analytically characterized the regions of parameters leading to viral persistence, in the form of *wt* only, of *wt* and defective segments, or segments only. We also defined the different types of relationships between *wt* and segments, and the presence or absence of selective pressure towards complementation, i.e., to witnessing the circulation of defective variants that may cooperatively reconstruct the whole genome. These findings were complemented with numerical simulations aimed at computing the prevalence of the different endemic states, and their probability of occurrence. As a result, we could identify under which ecological conditions would multipartitism be a successful adaptive strategy to new conditions and environments. Defective particles generated through replication errors would start circulating by hijacking the *wt* above a certain threshold that we calculated. Subsequently, a complementing set of variants might form. Once that situation is achieved, even a small advantage in transmissibility ( $\rho > 1$ ) would give an advantage to the multipartite form. This sequence of events represents a plausible, parsimonious evolutionary pathway to the rising and persistence of multipartite viruses.

We also analyzed the complex effect of heterogeneous topology, uncovering that while heterogeneity favors viral persistence in general, it gives a higher advantage to monopartite forms, by limiting the evolutionary potential of multipartitism as an adaptation strategy. Clearly our model lacks specific biological features that characterize different viruses, but this is a strength of the model, as it can be applied to a wide variety of settings with appropriate modifications. Though not quantitatively precise, we believe it provides an interesting qualitative picture of coexistence or substitution of different genomic architectures in realistic ecological environments. In this sense, we uncovered evidence that the topology of contacts along which viruses spread may be a contributing factor to explaining why multipartite viruses preferentially infect plants, and why their diversity flourished together with the expansion of agricultural practices.

## Methods

Our goal is to derive the critical surfaces of Eq. (2),(3),(4) from the equation driving the dynamics of the system, namely Eq. (S.1). We do that by starting from a simpler scenario,

and incrementally adding features, up to the full model. Specifically, the first step consists in solving the model with no differential degradation ( $\rho = 1$ ), no contact heterogeneity, and with only one segmented variant ( $v = 1$ ). In the second step we generalize the result to a generic  $v$ , and in the third one we allow for heterogeneous contacts. In the last step we add differential degradation. Finally, we solve the dynamics of satellites by modifying the  $v = 1$  model. A numerical validation of the critical surfaces is carried out in SI - Sec. 6.

$\lceil \text{wt} \rceil$ ,  $\lceil \text{all} \rceil$  are the only infectious compartments, with prevalence  $x_1, x_2$ , respectively. With neither differential degradation nor contact heterogeneity, Eq. (S.1) reduces to

$$\begin{cases} \dot{x}_1 = \lambda(1 - x_1 - x_2)x_1 + \lambda(1 - \lambda)(1 - x_1 - x_2)x_2 - \lambda x_1 x_2 - \mu x_1; \\ \dot{x}_2 = \lambda^2(1 - x_1 - x_2)x_2 + \lambda x_1 x_2 - \mu x_2. \end{cases} \quad (5)$$

By summing these equations, we find that the equation for the total prevalence ( $z \stackrel{\text{def}}{=} x_1 + x_2$ ) is  $\dot{z} = \lambda(1 - z)z - \mu z$ . This also follows from noticing that for  $v = 1$  the total prevalence is also the total *wt* prevalence (see SI - Sec. 5). This means that the total prevalence behaves as a standard SIS, for which we know the epidemic threshold  $T_1 = \{\lambda = \mu\}$ , and the equilibrium above it. In addition, we know that just above  $T_1$  we are in the *wt*-phase. Hence, we have ( $z_{wt} = 1 - \mu/\lambda, x_{2,eq} = 0$ ). Studying the stability of this equilibrium gives us  $T_2$ . Since the equation for  $z$  decouples from  $x_1$  and  $x_2$ , it is convenient to study the system in  $(z, x_2)$ . Studying the sign of the eigenvalues of the Jacobian reduces to studying  $\partial \dot{x}_2 / \partial x_2 < 0$  calculated in the equilibrium. This gives  $T_2 = \{\lambda = 2\mu/(1 + \mu)\}$ . The details of the calculation are reported in the SI - Sec. 1.

We now generalize the previous result to an arbitrary  $v$ , while still assuming that all hosts have the same contact rate, that we can set to one with no loss of generality. Eq. (S.1) simplifies to

$$\dot{x}_\nu = \sum_{\beta\gamma} \Lambda_{\nu\beta\sigma} x_\beta x_\sigma + \sum_{\beta} \Gamma_{\nu\beta} x_\beta \left(1 - \sum_{\sigma} x_\sigma\right) - \mu x_\nu, \quad (6)$$

whose Jacobian is

$$J_{\nu\beta} = \frac{\partial \dot{x}_\nu}{\partial x_\beta} = \sum_{\sigma} [\Lambda_{\nu(\beta\sigma)} - \Gamma_{\nu\sigma}] x_\sigma + \Gamma_{\nu\beta} \left(1 - \sum_{\sigma} x_\sigma\right) - \mu \delta_{\nu\beta}, \quad (7)$$

where  $\Lambda_{\nu(\beta\sigma)} = \Lambda_{\nu\beta\sigma} + \Lambda_{\nu\sigma\beta}$ . Firstly, we note that for  $v > 1$  the total prevalence, now defined as  $z = \sum_{\nu} x_\nu$ , no longer behaves like an SIS, due to the presence of the compartment  $\lceil \text{seg} \rceil$ . Indeed, one can show that, when summing over  $\nu$  in Eq. (S.1), the terms with  $\Lambda$  cancel out, as they pertain to interaction exclusively among infectious compartments, which by definition cannot change the total prevalence, and so all the contributions must cancel out. This is not the case however for the terms with  $\Gamma$ , so that the final equation is  $\dot{z} = (1 - z) \sum_{\beta} (\Gamma x)_{\beta} - \mu z$ , which does not decouple from  $x_\nu$ . Interestingly, despite this breaking of the SIS symmetry, which was crucial to solve the  $v = 1$  model, we can still prove that the values of  $T_1, T_2$  found for  $v = 1$  generalize to an arbitrary number of variants. We start from the first critical surface ( $T_1$ ). We compute the Jacobian of Eq. (S.8) in the **dfs**, i.e.,  $x_\beta = 0 \forall \beta$ . We get  $J^{(dfs)} = \Gamma - \mu$ . We now argue



$\Gamma$ , and therefore the Jacobian, is upper triangular, thanks to the specific ordering of the compartments that we introduced.  $\Gamma_{\nu\beta}$  is the rate at which a susceptible becomes a  $\lceil \nu \rceil$ , upon contact with a  $\lceil \beta \rceil$ . For this to happen ( $\Gamma_{\nu\beta} > 0$ ),  $\lceil \beta \rceil$  must contain at least all the viral species  $\lceil \nu \rceil$  contains. Hence, either  $\beta = \nu$  (diagonal term), or  $\beta > \nu$ . By the same reasoning, the diagonal terms are  $\Gamma_{\beta\beta} = \lambda^{\phi(\beta)}$ , where  $\phi(\beta)$  is the number of viral species in  $\lceil \beta \rceil$ , e.g.  $\phi(\lceil \text{wt} \rceil) = 1$ ,  $\phi(\lceil \text{all} \rceil) = v + 1$ . From these considerations, the spectrum of  $J^{(dfs)}$  is  $\{\lambda^{\phi(\beta)} - \mu; \forall \beta\}$ . Keeping in mind that  $\lambda < 1$ , we recover the first critical point:  $T_1 = \{\lambda = \mu\}$ .

Just above  $T_1$ ,  $\lceil \text{wt} \rceil$  is the only one with prevalence different than zero, hence it behaves like a standard SIS. Thanks to that we can compute Eq. (S.8) in the *wt*-phase, and its spectrum. From that we find that the second critical surface is the same as for  $v = 1$ . The details of the calculation are in SI - Sec. 2.

We now build on the previous section, by adding heterogeneous contact rates. We work in the widely-used degree-block approximation [22, 41, 23, 30, 24], assuming the contacts among agents are represented by an annealed network in which we assign each node a degree sampled from a power-law distribution with exponent  $\gamma$ :  $p_\gamma(k) = C_\gamma k^{-\gamma}$ , where  $C_\gamma$  is the normalization factor. As customary, we assume  $\gamma > 2$ , so that the average degree is defined in arbitrary large populations. In the framework of annealed networks it makes sense to interpret  $k$  as a discrete number. One could also interpret it as a (continuous) coupling potential. Either choice does not change the result found. We now directly compute the Jacobian of Eq. (S.1), reported in Eq. (S.16) of SI. The Jacobian is a matrix acting on a space which is the tensor product of the space of compartments, spanned by the Greek indices, and the space of degrees, spanned by the Latin indices. We can study its spectral properties on each space separately, using the results of the previous section for the space of compartments. The full derivation is reported in the SI - Sec. 3.

Differential degradation  $\rho > 1$  changes the matrices  $\Gamma, \Lambda$ , as reported in the SI - Sec. 4. The derivation is then similar to the case with  $\rho = 1$ .

Data in Fig. 4 are produced through stochastic spreading simulations. Starting with a population of  $N = 6000$ , we infected a hosts with *wt* and both segments ( $\lceil \text{all} \rceil$  for  $v = 2$ ), and let the virus spread. We use an adaptation of the Gillespie algorithm [42, 43], to model both contacts among hosts, and contagion and recovery events. For each parameter configuration, we simulate several (5000) iterations, and keep only those reaching an endemic state other than the disease-free state. We then use those iterations to compute both prevalences, and occurrence probabilities.

**Acknowledgments** We thank Michele Re Fiorentin for useful computational support. SM acknowledges financial support from Spanish MINECO and FEDER funds of the EU through grant ViralESS (FIS2014-57686-P). AA acknowledges financial support from Spanish MINECO (grant FIS2015-71582-C2-1), Generalitat de Catalunya ICREA Academia, and the James S. McDonnell Foundation grant #220020325.

# Supplementary Information

The notation used here is the same as the one introduced in the main text. Equations and figures of the main text are referenced with their number there, e.g., Fig. 1 and Eq. (2). Equations and figures of this supplementary material have a “S.” before their number, e.g., Fig. S.1 and Eq. (S.2).

We report here the equation describing the spread of the disease, corresponding to Eq. (1) of the main text:

$$\dot{x}_\nu^k = -\mu x_\nu^k + \frac{k}{\langle k \rangle} \sum_\beta \left( \sum_h h p_\gamma(h) x_\beta^h \right) \left[ \Gamma_{\nu\beta} \left( 1 - \sum_\gamma x_\gamma^k \right) + \sum_\gamma \Lambda_{\nu\beta\gamma} x_\gamma^k \right]. \quad (\text{S.1})$$

The terms in this equation are described in the main text. We remind that the Latin indices run on the degree, and Greek indices run over the  $2^v + 1$  compartments, that are ordered by increasing number of viral species they contain. Let us define as  $\phi$  the function that counts such number, so that  $\phi(\ulcorner \text{wt} \urcorner) = 1$  (just *wt*),  $\phi(\ulcorner 1 \urcorner) = 2$  (*wt* plus one variant),  $\phi(\ulcorner \text{seg} \urcorner) = v$  (all the variants),  $\phi(\ulcorner \text{all} \urcorner) = v + 1$ , and so on. The ordering is such that  $\alpha > \beta \Rightarrow \phi(\ulcorner \alpha \urcorner) \geq \phi(\ulcorner \beta \urcorner)$ .

## S.1 Model $v = 1$

Here we consider  $v = 1$ , homogeneous contacts, and no differential degradation. Let  $x_1, x_2$  be the prevalence of  $\ulcorner \text{wt} \urcorner, \ulcorner \text{all} \urcorner$ , respectively. Equation (S.1) reduces to

$$\begin{cases} \dot{x}_1 = -\mu x_1 + \lambda(1 - x_1 - x_2)x_1 + \lambda(1 - \lambda)(1 - x_1 - x_2)x_2 - \lambda x_1 x_2; \\ \dot{x}_2 = -\mu x_2 + \lambda^2(1 - x_1 - x_2)x_2 + \lambda x_1 x_2. \end{cases} \quad (\text{S.2})$$

As explained in the main text, the equation of the total prevalence  $z = x_1 + x_2$  decouples (see also Sec. S.5). It is thus convenient to consider the system in  $(z, x_2)$ :

$$\begin{cases} \dot{z} = \lambda(1 - z)z - \mu z \\ \dot{x}_2 = \lambda^2(1 - z)x_2 + \lambda(z - x_2)x_2 - \mu x_2. \end{cases} \quad (\text{S.3})$$

As the equation for  $z$  decouples from  $x_2$ , the Jacobian is lower triangular:

$$J = \begin{pmatrix} -\mu + \lambda(1 - 2z) & 0 \\ \lambda(1 - \lambda)x_2 & \lambda^2(1 - z) + \lambda(z - 2x_2) - \mu \end{pmatrix}. \quad (\text{S.4})$$

The spectrum of  $J$  is thus given by its diagonal elements. In order to get  $T_1$ , i.e., the epidemic threshold, we need to study the spectrum of  $J$  computed in the disease-free state ( $z = x_2 = 0$ ):

$$J^{(dfs)} = \begin{pmatrix} -\mu + \lambda & 0 \\ 0 & \lambda^2 - \mu \end{pmatrix}. \quad (\text{S.5})$$

From this we see that if  $\lambda > \mu$  the  $dfs$  is no longer stable. Hence  $T_1 = \{\lambda = \mu\}$ . One could guess this without calculations from the equation in  $z$ , which tells us that the total prevalence behaves like an SIS. In order to find  $T_2$  we now study the stability of the equilibrium where only  $wt$  is circulating (hosts in  $\lceil \mathbf{wt} \rceil$  are present, not in  $\lceil \mathbf{all} \rceil$ ). This is the equilibrium  $\mathbf{wt}$  defined in the main text, and it is a pure SIS model for the compartment  $\lceil \mathbf{wt} \rceil$ . The value of the prevalence is ( $z = 1 - \mu/\lambda, x_2 = 0$ ), as the SIS prescribes. The Jacobian in this equilibrium point is

$$J^{(\mathbf{wt})} = \begin{pmatrix} \mu - \lambda & 0 \\ 0 & \lambda(1 + \mu) - 2\mu \end{pmatrix}. \quad (\text{S.6})$$

The first eigenvalue is always negative, as we are above  $T_1$ . The second one is negative iff  $(1 + \mu)\lambda < 2\mu$ . As a result, we get that  $T_2 = \{\lambda = 2\mu/(1 + \mu)\}$ .

## S.2 Generic number of variants $v$

Assuming a generic number of variants, and homogeneous contacts, Eq. (S.1), and its Jacobian, are

$$\dot{x}_\nu = \sum_{\beta\sigma} \Lambda_{\nu\beta\sigma} x_\beta x_\sigma + \sum_{\beta} \Gamma_{\nu\beta} x_\beta \left(1 - \sum_{\sigma} x_\sigma\right) - \mu x_\nu; \quad (\text{S.7})$$

$$J_{\nu\beta} = \frac{\partial \dot{x}_\nu}{\partial x_\beta} = \sum_{\sigma} [\Lambda_{\nu(\beta\sigma)} - \Gamma_{\nu\sigma}] x_\sigma + \Gamma_{\nu\beta} \left(1 - \sum_{\sigma} x_\sigma\right) - \mu \delta_{\nu\beta}, \quad (\text{S.8})$$

with  $\Lambda_{\nu(\beta\sigma)} = \Lambda_{\nu\beta\sigma} + \Lambda_{\nu\sigma\beta}$ . They correspond to Eq. (6) and Eq. (7) of the main text.

As in the case  $v = 1$ , we use the Jacobian (Eq. (S.8)) to study the stability of two equilibria. The first one is the **dfs** ( $x_\nu = 0$ ), whose analysis will give  $T_1$ . The second one is **wt**:  $x_1 = 1 - \mu/\lambda$ ,  $x_\nu = 0$  for  $\nu > 1$ , and will give  $T_2$ . We remind that, given the ordering we use, the index  $\nu = 1$  refers to the compartment  $\lceil \mathbf{wt} \rceil$ , which is indeed the only one with non-zero prevalence in the  $wt$ -phase equilibrium. We study the stability of the former directly in the main text, so we will now directly proceed to the latter.

The Jacobian computed in **wt** is

$$J_{\nu\beta}^{(\mathbf{wt})} = \left(1 - \frac{\mu}{\lambda}\right) (\Lambda_{\nu(\beta 1)} - \Gamma_{\nu 1}) + \frac{\mu}{\lambda} \Gamma_{\nu\beta} - \mu \delta_{\nu\beta}. \quad (\text{S.9})$$

We can write it in matrix form by defining the following matrices:  $(\Lambda)_{\nu\beta} = \Lambda_{\nu(\beta 1)}$ ,  $(\tilde{\Gamma})_{\nu\beta} = \Gamma_{\nu 1}$ . The result is

$$J^{(\mathbf{wt})} = \Gamma - \mu + \left(1 - \frac{\mu}{\lambda}\right) (\Lambda - \Gamma - \tilde{\Gamma}). \quad (\text{S.10})$$

$\tilde{\Gamma}$  has all the entries equal to  $\Gamma_{11} = \lambda$  in the first row, and all others zero. This is because  $\Gamma_{\nu 1}$  encodes the interactions that change the prevalence of the  $\nu$ -th compartment by acting with  $\lceil \mathbf{wt} \rceil$  on the susceptible state. Hence  $\nu$  itself can refer only to  $\lceil \mathbf{wt} \rceil$ , and only  $wt$  is transmitting, thus the value  $\lambda$ . We now wish to show that  $\Lambda$  is block-upper-triangular. One diagonal block,  $\Lambda_1$ , encompasses the indices  $\beta = 1, \dots, 2^v - 1$ , while the other,  $\Lambda_2$ , the remaining  $\beta = 2^v, 2^v + 1$ :

$$\Lambda = \left( \begin{array}{c|c} \Lambda_1 [2^v - 1 \times 2^v - 1] & \dots \\ \hline 0 & \Lambda_2 [2 \times 2] \end{array} \right). \quad (\text{S.11})$$

The lower left block is clearly zero, because the transitions that change the prevalence of  $\lceil \mathbf{seg} \rceil, \lceil \mathbf{all} \rceil$  by acting on  $\lceil \mathbf{wt} \rceil$  with a compartment other than  $\lceil \mathbf{seg} \rceil, \lceil \mathbf{all} \rceil$ , or vice versa, are not possible. The block  $\Lambda_1$  is upper diagonal, and we can show this with a reasoning similar to the one for  $\Gamma$  in the main text. First of all,  $\Lambda_{1,11} = 0$  as no term  $x_1^2$  exists in the equations. We then consider the transitions  $\lceil \alpha \rceil \lceil \mathbf{wt} \rceil \rightarrow \lceil \alpha \rceil \lceil \beta \rceil$ , with  $1 < \alpha, \beta \leq 2^v - 1$ . It must be that  $\phi(\alpha) \geq \phi(\beta)$ , implying  $\alpha \geq \beta$ . Furthermore, the diagonal elements are  $\Lambda_{1,\alpha\alpha} = \lambda^{\phi(\alpha)-1}$ , as one needs to transmit all the segmented variants  $\lceil \alpha \rceil$  contains, but not  $wt$ . Finally, the transitions  $\lceil \mathbf{wt} \rceil \lceil \alpha \rceil \rightarrow \lceil \mathbf{wt} \rceil \lceil \beta \rceil$  are not possible, as all the compartments considered already contain the  $wt$ . This proves the upper diagonal shape. The block  $\Lambda_2$  does not change in dimension with  $v$ , and so it can be computed explicitly by analyzing the four possible reactions between  $\lceil \mathbf{seg} \rceil, \lceil \mathbf{all} \rceil$ . Summing up, the matrices involved have the following form:

$$\Gamma = \left( \begin{array}{cccccc|cc} \lambda & \blacksquare & \dots & \blacksquare & \dots & \blacksquare & \blacksquare & \blacksquare \\ 0 & \lambda^2 & \dots & \blacksquare & \dots & \blacksquare & \blacksquare & \blacksquare \\ \vdots & \vdots & \dots & \vdots & \dots & \vdots & \vdots & \vdots \\ 0 & 0 & \dots & \lambda^n & \dots & \blacksquare & \blacksquare & \blacksquare \\ \vdots & \vdots & \dots & \vdots & \dots & \vdots & \vdots & \vdots \\ 0 & 0 & \dots & 0 & \dots & \lambda^v & \blacksquare & \blacksquare \\ \hline 0 & 0 & \dots & 0 & \dots & 0 & \lambda^v & \lambda^v(1-\lambda) \\ 0 & 0 & \dots & 0 & \dots & 0 & 0 & \lambda^{v+1} \end{array} \right), \quad (\text{S.12})$$

$$\Lambda = \left( \begin{array}{cccccc|cc} 0 & \blacksquare & \dots & \blacksquare & \dots & \blacksquare & \blacksquare & \blacksquare \\ 0 & \lambda & \dots & \blacksquare & \dots & \blacksquare & \blacksquare & \blacksquare \\ \vdots & \vdots & \dots & \vdots & \dots & \vdots & \vdots & \vdots \\ 0 & 0 & \dots & \lambda^{n-1} & \dots & \blacksquare & \blacksquare & \blacksquare \\ \vdots & \vdots & \dots & \vdots & \dots & \vdots & \vdots & \vdots \\ 0 & 0 & \dots & 0 & \dots & \lambda^{v-1} & \blacksquare & \blacksquare \\ \hline 0 & 0 & \dots & 0 & \dots & 0 & -\lambda & 0 \\ 0 & 0 & \dots & 0 & \dots & 0 & \lambda(1+\lambda^{v-1}) & \lambda^v \end{array} \right), \quad (\text{S.13})$$

$$\tilde{\Gamma} = \left( \begin{array}{cccccc|cc} \lambda & \lambda & \cdots & \lambda & \cdots & \lambda & \lambda & \lambda \\ 0 & 0 & \cdots & 0 & \cdots & 0 & 0 & 0 \\ \vdots & \vdots & \cdots & \vdots & \cdots & \vdots & \vdots & \vdots \\ 0 & 0 & \cdots & 0 & \cdots & 0 & 0 & 0 \\ \vdots & \vdots & \cdots & \vdots & \cdots & \vdots & \vdots & \vdots \\ 0 & 0 & \cdots & 0 & \cdots & 0 & 0 & 0 \\ \hline 0 & 0 & \cdots & 0 & \cdots & 0 & 0 & 0 \\ 0 & 0 & \cdots & 0 & \cdots & 0 & 0 & 0 \end{array} \right), \quad (\text{S.14})$$

where  $2 \leq n \leq v$ , and the symbol “■” marks values that are not necessary to our computation. By putting Eq. (S.12),(S.13),(S.14) into Eq. (S.10) we realize that  $J^{(\text{wt})}$  has the same block structure, and can compute its eigenvalues. The stability condition then translates into the following system:

$$\begin{cases} \mu - \lambda < 0 \\ \lambda^n - \mu + \lambda^{n-1} \left(1 - \frac{\mu}{\lambda}\right) (1 - \lambda) < 0 \\ \lambda^v - \mu < 0 \\ \lambda (\mu \lambda^{v-1} - 1) < 0 \end{cases}. \quad (\text{S.15})$$

The first equation is always true, as we are above  $T_1$ . The second one, for  $n = 2$ , is true when  $\lambda < 2\mu/(1 + \mu)$ . Then, if this holds, one can show that all the following hold. As a result, we get to  $T_2 = \{\lambda = 2\mu/(1 + \mu)\}$ .

### S.3 Heterogeneous contacts

We now address the fully general equation driving the system: Eq (S.1). We assume here  $k$  to be discrete-valued. One can prove that the whole derivation holds in the continuous case, too. The general form of the Jacobian (Eq. (S.1)) becomes

$$\begin{aligned} J_{\nu\alpha}^{km} = \frac{\partial \dot{x}_{\nu}^k}{\partial x_{\alpha}^m} = & \frac{k}{\langle k \rangle} m p_{\gamma}(m) \left[ \Gamma_{\nu\alpha} \left( 1 - \sum_{\gamma} x_{\gamma}^k \right) + \gamma \Lambda_{\nu\alpha\gamma} x_{\gamma}^k \right] + \\ & + \delta^{km} \left[ -\mu \delta_{\nu\alpha} + \frac{k}{\langle k \rangle} \sum_{\beta, h} h p_{\gamma}(h) x_{\beta}^h (\Lambda_{\nu\beta\alpha} - \Gamma_{\nu\beta}) \right]. \end{aligned} \quad (\text{S.16})$$

This matrix acts on the space  $\mathcal{G} \otimes \mathcal{H}$ , where  $\mathcal{G}$  is the usual  $(2^v + 1)$ -dimensional space spanned by the compartments, and  $\mathcal{H}$  is an  $\infty$ -dimensional separable Euclidean space spanned by the discrete degrees (or contact rates). For this reason, we can study the spectrum of  $J$  on the compartment sector, and the degree sector, one at the time.

#### S.3.1 $T_1$

On the  $df$ s, the Jacobian reads

$$J_{\nu\alpha}^{km} \Big|^{(\text{wt})} = C_{\gamma} \frac{k m^{1-\gamma}}{\langle k \rangle} \Gamma_{\nu\alpha} - \mu \delta^{km} \delta_{\nu\alpha}. \quad (\text{S.17})$$

In Sec. S.2 we already have examined both  $\Gamma$  and  $\Lambda$  thoroughly. Hence, we can say that the principal eigenvalue of  $\Gamma$  is  $\lambda - \mu$ , corresponding to some eigenvector  $v$ . If one defines the vector  $\kappa$  on  $\mathcal{H}$  as simply the sequence of positive natural numbers  $\kappa = (1 \ 2 \ 3 \ \dots)$ , then one can show that  $\kappa \otimes v$  is the principal eigenvector of  $J|^{(\text{wt})}$ , with eigenvalue  $\langle k^2 \rangle \lambda / \langle k \rangle - \mu$ . From this we find  $T_1 = \{\lambda = \hat{\mu}\}$ .

### S.3.2 $T_2$

Let us call  $z^k \stackrel{\text{def}}{=} x_1^k$ . The **wt** equilibrium will be some  $z^k > 0$ , and  $x_\nu^k = 0 \ \forall \nu > 1$ . This leads to (dropping the superscript **wt** from now on)

$$J_{\nu\alpha}^{km} = \frac{mp_\gamma(m)}{\langle k \rangle} k [\Gamma_{\nu\alpha}(1 - z^k) + \Lambda_{\nu\alpha 1} z^k] + \quad (\text{S.18})$$

$$+ \delta^{km} \left[ -\mu \delta_{\nu\alpha} + k \langle z \rangle_{\gamma-1} (\Lambda_{\nu 1\alpha} - \Gamma_{\nu 1}) \right], \quad (\text{S.19})$$

where  $\langle z \rangle_\sigma$  is the average of  $z^k$  computed with  $p_\sigma(k)$ :  $\langle z \rangle_\sigma \stackrel{\text{def}}{=} C_\sigma \sum_k z^k k^{-\sigma}$ . By using the findings in Sec. S.2, we know that, in the compartment sector, the relevant (dominant) eigenvalue is the entry  $\nu = \alpha = 2$ . Hence, we can directly compute the Jacobian for these values, and deal with the degree sector:

$$J^{km} = -\mu \delta^{km} + \frac{mp_\gamma(m)}{\langle k \rangle} k [\lambda^2(1 - z^k) + \lambda z^k]. \quad (\text{S.20})$$

We now define two vectors (in  $\mathcal{H}$ ):  $\Omega_k \stackrel{\text{def}}{=} kp_\gamma(k) / \langle k \rangle$ , and  $\Psi_k \stackrel{\text{def}}{=} k (\lambda^2 + \lambda(1 - \lambda)z^k)$ . With them we can rewrite  $J^{km}$ :

$$J = -\mu + \Psi \Omega^T. \quad (\text{S.21})$$

The principal eigenvector of  $J$  is  $\Psi$ , and the corresponding eigenvalue is  $-\mu + \Omega^T \Psi$ . By computing it, and setting it to zero, we recover the equation for the critical point:

$$\lambda + (1 - \lambda) \langle z \rangle_{\gamma-2} = \frac{\langle k \rangle}{\langle k^2 \rangle} \frac{\mu}{\lambda}. \quad (\text{S.22})$$

The last piece of the puzzle is computing the term  $\langle z \rangle_{\gamma-2}$ . We define the following function:

$$g(a, x) \stackrel{\text{def}}{=} \sum_{k=1}^{\infty} \frac{k^{-a}}{1 + xk}. \quad (\text{S.23})$$

For this function, one can prove the following recursion relation:

$$xg(a-1, x) = \zeta(a) - g(a, x) \quad (\text{S.24})$$

(derivation not shown here). Now, from [22] we know that the prevalence  $z^k$  of a SIS model obeys the following equation:

$$z^k = \frac{\lambda \langle z \rangle_{\gamma-1}}{\mu + \lambda \langle z \rangle_{\gamma-1}}. \quad (\text{S.25})$$

We apply  $C_{\gamma-1} \sum_k k^{1-\gamma}$  to both sides of this equations, and get

$$g\left(\gamma - 2, \frac{\lambda}{\mu} \langle z \rangle_{\gamma-1}\right) = \frac{\mu}{\lambda C_{\gamma-1}}. \quad (\text{S.26})$$

We then apply  $C_{\gamma-2} \sum_k k^{2-\gamma}$ , and get

$$\langle z \rangle_{\gamma-2} = \langle z \rangle_{\gamma-1} \frac{\lambda}{\mu} g\left(\gamma - 3, \frac{\lambda}{\mu} \langle z \rangle_{\gamma-1}\right). \quad (\text{S.27})$$

Moreover, we notice that the moments of the degree distribution can be expressed in terms of the normalization constants as follows:

$$\langle k^n \rangle = \frac{C_\gamma}{C_{\gamma-n}}. \quad (\text{S.28})$$

By combining Eq. (S.23),(S.26),(S.27),(S.28) we can get to a closed-form solution for  $\langle z \rangle_{\gamma-2}$ :

$$\langle z \rangle_{\gamma-2} = 1 - \frac{\langle k \rangle}{\langle k^2 \rangle} \frac{\mu}{\lambda}. \quad (\text{S.29})$$

Finally, by putting this inside Eq. (S.22), we get to  $T_2 = \{\lambda = 2\hat{\mu}/(1 + \hat{\mu})\}$ .

## S.4 Enhanced segment transmissibility

Segmented variants now transmit with a probability  $\rho\lambda$ , with  $\rho \geq 1$ , where  $\lambda$  is the transmissibility of *w.t.* Let us examine how the interaction matrices change according to this. Matrix  $\tilde{\Gamma}$  in Eq. (S.14) does not change, while matrix  $\Gamma$  Eq. (S.12), and  $\Lambda$  in Eq. (S.13), change as follows:

$$\Gamma = \left( \begin{array}{cccccc|cc} \lambda & \blacksquare & \cdots & \blacksquare & \cdots & \blacksquare & \blacksquare & \blacksquare \\ 0 & \rho\lambda^2 & \cdots & \blacksquare & \cdots & \blacksquare & \blacksquare & \blacksquare \\ \vdots & \vdots & \cdots & \vdots & \cdots & \vdots & \vdots & \vdots \\ 0 & 0 & \cdots & \rho^{n-1}\lambda^n & \cdots & \blacksquare & \blacksquare & \blacksquare \\ \vdots & \vdots & \cdots & \vdots & \cdots & \vdots & \vdots & \vdots \\ 0 & 0 & \cdots & 0 & \cdots & \rho^{v-1}\lambda^v & \blacksquare & \blacksquare \\ \hline 0 & 0 & \cdots & 0 & \cdots & 0 & (\rho\lambda)^v & (\rho\lambda)^v(1-\lambda) \\ 0 & 0 & \cdots & 0 & \cdots & 0 & 0 & \rho^v\lambda^{v+1} \end{array} \right), \quad (\text{S.30})$$

$$\Lambda = \left( \begin{array}{cccccc|cc} 0 & \blacksquare & \cdots & \blacksquare & \cdots & \blacksquare & \blacksquare & \blacksquare \\ 0 & \rho\lambda & \cdots & \blacksquare & \cdots & \blacksquare & \blacksquare & \blacksquare \\ \vdots & \vdots & \cdots & \vdots & \cdots & \vdots & \vdots & \vdots \\ 0 & 0 & \cdots & (\rho\lambda)^{n-1} & \cdots & \blacksquare & \blacksquare & \blacksquare \\ \vdots & \vdots & \cdots & \vdots & \cdots & \vdots & \vdots & \vdots \\ 0 & 0 & \cdots & 0 & \cdots & (\rho\lambda)^{v-1} & \blacksquare & \blacksquare \\ \hline 0 & 0 & \cdots & 0 & \cdots & 0 & -\lambda & 0 \\ 0 & 0 & \cdots & 0 & \cdots & 0 & \lambda + (\rho\lambda)^v & (\rho\lambda)^v \end{array} \right), \quad (\text{S.31})$$

The spectrum of  $J^{dfs} = \Gamma - \mu$  then gives the first critical point. We find two regimes. For  $\rho < \mu^{-\frac{v-1}{v}}$ , we find the usual  $T_1 = \{\lambda = \mu\}$ . For  $\rho > \mu^{-\frac{v-1}{v}}$  a different critical point emerges:  $T_s = \left\{ \lambda = (\mu)^{1/v} / \rho \right\}$ . This means that if transmissibility is enhanced enough, the compartment  $\lceil \text{seg} \rceil$  spreads alone as an SIS, and  $T_s$  is its epidemic threshold.

In the regime  $\rho < \mu^{-\frac{v-1}{v}}$  we can find the new  $T_2 = \left\{ \lambda = \frac{1+\rho}{\rho} \frac{\mu}{1+\mu} \right\}$ , with the same derivation as in Sec. S.2. Analogously we can add heterogeneous contact rates, solving the degree sector as in Sec. S.3, finding the correction  $\hat{\mu}$  as before.

## S.5 Total prevalence of the wild-type virus

Total prevalence of the *wt* can be computed analytically in the homogeneous case. In order to prove that, we consider Eq. S.7. For convenience, we define  $z = \sum_{\alpha} x_{\alpha} - x_{seg}$ , which is the total prevalence of the *wt*. Primed summation symbols ( $\sum'_{\nu}$ ) mean  $\nu$  runs over all the compartments but  $\lceil \text{seg} \rceil$ . We apply  $\sum'_{\nu}$  to both sides of Eq. S.7, getting

$$\dot{z} = -\mu z + \sum_{\alpha\beta} x_{\alpha} x_{\beta} \left( \sum'_{\nu} \Lambda_{\nu\alpha\beta} \right) + (1 - z - x_{seg}) \sum_{\alpha} x_{\alpha} \left( \sum'_{\nu} \Gamma_{\nu\alpha} \right). \quad (\text{S.32})$$

The term containing  $\Lambda_{\nu\alpha\beta}$  can be computed using the fact that  $\sum_{\nu} \Lambda_{\nu\alpha\beta} = 0$ . This is due to the fact that the number of hosts is conserved, and  $\Lambda_{\nu\alpha\beta}$  encodes interactions only between infected compartments. As a result,  $\sum'_{\nu} \Lambda_{\nu\alpha\beta} = -\Lambda_{seg,\alpha\beta}$ . Moreover, one can show that  $\Lambda_{seg,\alpha\beta} = -\lambda \delta_{\beta,seg} (1 - \delta_{\alpha,seg})$ . The term  $\sum'_{\nu} \Gamma_{\nu\alpha}$  is the probability of  $\alpha$  generating a  $\nu \neq seg$  by infecting a susceptible. This is just the probability of transmitting the *wt*, because all the other probabilities cancel out. Hence,  $\sum'_{\nu} \Gamma_{\nu\alpha} = \lambda(1 - \delta_{\alpha,seg})$ . By inserting these two terms in Eq. (S.32), one gets

$$\dot{z} = -\mu z + \lambda(1 - z)z, \quad (\text{S.33})$$

which decouples from the other variables, and represents a pure SIS. As a result, the endemic total prevalence of the *wt* in case of homogeneous networks is always  $z = 1 - \mu/\lambda$ .

## S.6 Numerical validation of the critical surfaces

In order to validate our theoretical prediction of the phase space, we simulate the spread of a multipartite virus on a plant population. The estimate of the critical surfaces requires computing the endemic states, corresponding to the different phases. To do that, we use the quasistationary state method [44, 45]. In its original formulation for an SIS model, the quasistationary state method relies on forcing the system out of the disease-free state. Every time the simulation produces a fully susceptible population, one inputs an active configuration previously visited by the system. With multipartite viruses, however, there is an additional challenge, represented by the fact that the disease-free state is not the only absorbing state. Every time the system becomes free of a specific variant (or *wt*) disappears from the system, it will be free of it forever. Hence, we force the system out of any state that does not contain all the  $v$  variants and the *wt*. The result of the simulations is shown in Fig. S.1.



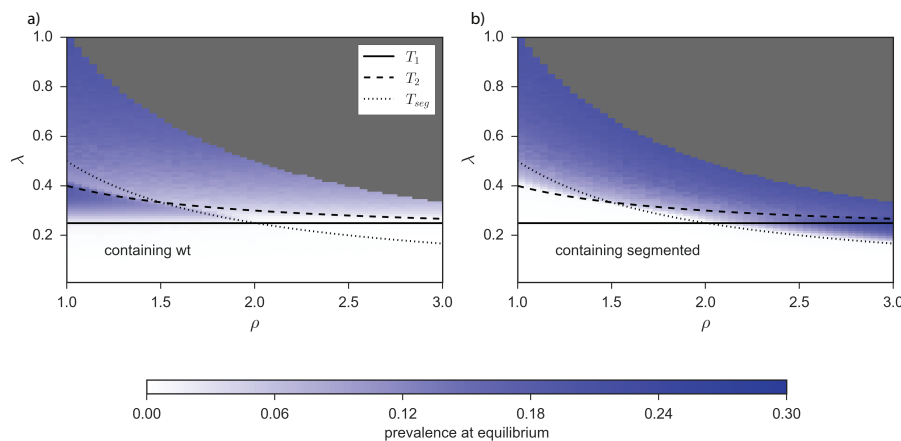


**Figure S.1:** This figure represents the numerical validation of Fig. 2(E) of the main text. Prevalence of the *wt* (A) and the segmented variants (B) are computed through stochastic simulations and plotted here. The solid, dashed and dotted lines represent  $T_1$ ,  $T_2$ ,  $T_s$ , respectively.

## References

- [1] R M Lister. Possible relationships of virus-specific products of tobacco rattle virus infections. *Virology*, 28:350–353, 1966.
- [2] Anne Sicard, Yannis Michalakakis, Serafín Gutiérrez, and Stéphane Blanc. The Strange Lifestyle of Multipartite Viruses. *PLoS pathogens*, 12(11):e1005819, 2016.
- [3] Mattia Dall’Ara, Claudio Ratti, Salah E Bouzoubaa, and David Gilmer. Ins and Outs of multipartite positive-strand {RNA} plant viruses: Packaging versus systemic spread. *Viruses*, 8:228, 2016.
- [4] Beilei Wu, Mark P Zwart, Jesús A Sánchez-Navarro, and Santiago F Elena. Within-host Evolution of Segments Ratio for the Tripartite Genome of Alfalfa Mosaic Virus. *Scientific Reports*, 7:5004, 2017.
- [5] Adriana Lucía-Sanz and Susanna C. Manrubia. Multipartite viruses: adaptive trick or evolutionary treat? *npj Systems Biology and Applications*, 3(1):34, 2017.
- [6] Pedro Moreno, Silvia Ambrós, Maria R Albiach-Martí, José Guerri, and Leandro Peña. Citrus tristeza virus: a pathogen that changed the course of the citrus industry. *Molecular Plant Pathology*, 9(2):251–268.
- [7] A. J. Gibbs, D. Fargette, F. Garcia-Arenal, and M. J. Gibbs. Time - the emerging dimension of plant virus studies. *Journal of General Virology*, 91(1):13–22, jan 2010.
- [8] Alice S Huang. Defective interfering viruses. *Annu. Rev. Microbiol.*, 27:101–118, 1973.
- [9] J Perrault. Origin and replication of defective interfering particles. *Curr. Top. Microbiol. Immunol.*, 93:151—207, 1981.

- [10] Sondra Schlesinger. The Generation and Amplification of Defective Interfering RNAs. In Esteban Domingo, John Hollard, and Paul Ahlquist, editors, *RNA Genetics: Volume II: Retroviruses, Viroids, and RNA Recombination*, pages 175–194. CRC Press, 2018.
- [11] Juan García-Arriaza, Susanna C Manrubia, Miguel Toja, Esteban Domingo, and Cristina Escarmís. Evolutionary transition toward defective {RNAs} that are infectious by complementation. *Journal of Virology*, 78:11678–11685, 2004.
- [12] Jaime Iranzo and Susanna C. Manrubia. Evolutionary dynamics of genome segmentation in multipartite viruses. *Proceedings of the Royal Society B: Biological Sciences*, 279(1743):3812–3819, 2012.
- [13] Lin Chao. Levels of selection, evolution of sex in {RNA} viruses and the origin of life. *J. Theor. Biol.*, 153:229–246, 1991.
- [14] J Pressing and D C Reanne. Divided genomes and intrinsic noise. *J. Mol. Evol.*, 20:135–146, 1984.
- [15] Sean Nee and John M Maynard-Smith. The evolutionary biology of molecular parasites. *Parasitology*, 100:S5—S18, 1990.
- [16] Samuel Ojosnegros, Juan García-Arriaza, Cristina Escarmís, Susanna C Manrubia, Celia Perales, Armando Arias, Mauricio García-Mateu, and Esteban Domingo. Viral Genome Segmentation Can Result from a Trade-Off between Genetic Content and Particle Stability. *PLoS Genet.*, 7:e1001344, 2011.
- [17] Anne Sicard, Jean-Louis Zeddam, Michel Yvon, Yannis Michalakis, Serafin Gutiérrez, and Stéphane Blanc. Circulative Nonpropagative Aphid Transmission of Nanoviruses: an Oversimplified View. *Journal of virology*, 89(19):9719–26, 2015.
- [18] B Moury, F Fabre, and R Senoussi. Estimation of the number of virus particles transmitted by an insect vector. *Proceedings of the National Academy of Sciences of the United States of America*, 104(45):17891–17896, 2007.
- [19] Susanna C. Manrubia, Esteban Domingo, and Ester Lázaro. Pathways to extinction: beyond the error threshold. *Phil. Tans. R. Soc.*, 365(1548):1943–1952, 2010.
- [20] Catherine K Denny and Scott E Nielsen. Spatial Heterogeneity of the Forest Canopy Scales with the Heterogeneity of an Understory Shrub Based on Fractal Analysis. *Forests*, 8:146, 2017.
- [21] Billie Leff, Navin Ramankutty, and Jonathan A Foley. Geographic distribution of major crops across the world. *Global Biogeochem. Cycles*, 18:GB1009, 2004.
- [22] Romualdo Pastor-Satorras and Alessandro Vespignani. Epidemic spreading in scale-free networks. *Phys. Rev. Lett.*, 86(14):3200–3203, 2001.
- [23] M E J Newman. Spread of epidemic disease on networks. *Phys. Rev. E*, 66(1):16128, 2002.

- [24] Romualdo Pastor-Satorras, Claudio Castellano, Piet Van Mieghem, and Alessandro Vespignani. Epidemic processes in complex networks. *Reviews of Modern Physics*, 87(3):925–979, 2015.
- [25] P Rohani, C J Green, N B Mantilla-Beniers, and B T Grenfell. Ecological interference between fatal diseases. *Nature*, 422(6934):885–888, 2003.
- [26] M E J Newman. Threshold effects for two pathogens spreading on a network. *Physical Review Letters*, 95(10):1–4, 2005.
- [27] Laith J Abu-Raddad, Padmaja Patnaik, and James G Kublin. Dual Infection with HIV and Malaria Fuels the Spread of Both Diseases in Sub-Saharan Africa. *Science*, 314(5805):1603 LP – 1606, dec 2006.
- [28] Brian Karrer and M E J Newman. Competing epidemics on complex networks. *Physical Review E - Statistical, Nonlinear, and Soft Matter Physics*, 84(3):1–12, 2011.
- [29] Chiara Poletto, Sandro Meloni, Vittoria Colizza, Yamir Moreno, and Alessandro Vespignani. Host Mobility Drives Pathogen Competition in Spatially Structured Populations. *PLOS Computational Biology*, 9(8):1–12, 2013.
- [30] Alain Barrat, Marc Barthélemy, and Alessandro Vespignani. *Dynamical Processes on Complex Networks*. Cambridge University Press, 2008.
- [31] Rachel S Meyer and Michael D Purugganan. Evolution of crop species: genetics of domestication and diversification. *Nat. Rev. Genet.*, 14:840–852, 2013.
- [32] F J O’Neill, E B Maryon, and D Carroll. Isolation and characterization of defective simian virus 40 genomes which complement for infectivity. *J. Virol.*, 43:18–25, 1982.
- [33] U Geigenmüller-Gnirke, B Weiss, R Wright, and S Schlesinger. Complementation between Sindbis viral {RNA}s produces infectious particles with a bipartite genome. 88:3253, 1991.
- [34] K H Kim, K Narayanan, and S Makino. Assembled coronavirus from complementation of two defective interfering {RNA}s. *J. Virol.*, 71:3922, 1997.
- [35] B Kassanis. Properties and behaviour of a virus depending for its multiplication on another. *J. Gen. Microbiol.*, 27:477–488, 1962.
- [36] Muhammad Shah Nawaz-ul Rehman and Claude M Fauquet. Evolution of geminiviruses and their satellites. *FEBS Lett.*, 583:1825–1832, 2009.
- [37] Bernard La Scola, Christelle Desnues, Isabelle Pagnier, Catherine Robert, Lina Barrasi, Ghislain Fournous, Michèle Merchat, Marie Suzan-Monti, Patrick Forterre, Eugene Koonin, and Didier Raoult. The virophage as a unique parasite of the giant mimivirus. *Nature*, 455:100–104, 2008.

- [38] Ricardo Flores, Douglas Grubb, Amine Elleuch, María-Ángeles Nohales, Sonia Delgado, and Selma Gago. Rolling-circle replication of viroids, viroid-like satellite RNAs and hepatitis delta virus: Variations on a theme. *RNA Biology*, 8:200–206, 2011.
- [39] Jonathan D Wren, Marilyn J Roossinck, Richard S Nelson, Kay Scheets, Michael W Palmer, and Ulrich Melcher. Plant virus biodiversity and ecology. *PLoS Biology*, 4:314–315, 2006.
- [40] S Alizon, A Hurford, N Mideo, and M Van Baalen. Virulence evolution and the trade-off hypothesis: history, current state of affairs and the future. *Journal of Evolutionary Biology*, 22:245–259, 2009.
- [41] Romualdo Pastor-Satorras and Alessandro Vespignani. Epidemic dynamics and endemic states in complex networks. *Physical Review E*, 63:066117, 2001.
- [42] J L Doob. Topics in the theory of Markoff chains. *Transactions of the American Mathematical Society*, 52(1):37, jan 1942.
- [43] Christian L. Vestergaard and Mathieu Géniois. Temporal Gillespie Algorithm: Fast Simulation of Contagion Processes on Time-Varying Networks. *PLoS Computational Biology*, 11(10):1–28, 2015.
- [44] Silvio C Ferreira, Ronan S Ferreira, Claudio Castellano, and Romualdo Pastor-Satorras. Quasistationary simulations of the contact process on quenched networks. *Phys. Rev. E*, 84(6):66102, dec 2011.
- [45] Silvio C Ferreira, Claudio Castellano, and Romualdo Pastor-Satorras. Epidemic thresholds of the susceptible-infected-susceptible model on networks: A comparison of numerical and theoretical results. *Phys. Rev. E*, 86(4):41125, oct 2012.